JOURNAL OF MATERIALS SCIENCE 29 (1994) 6379–6396

The preparation and properties of some lithium borate based glasses

I. W. DONALD, B. L. METCALFE, D. J. BRADLEY, M. J. C. HILL, J. L. McGRATH, A. D. BYE
Atomic Weapons Establishment, Aldermaston, Berkshire, UK RG7 4PR

The preparation and properties of lithium borate based glasses are described. The properties which were monitored included the glass-forming ability, the thermal stability, the chemical durability and the mechanical behaviour. Methods which were used in an attempt to improve the mechanical properties of these glasses are also discussed, including controlled crystallization, chemical ion-exchange and fibre reinforcement. The strongest glass, which had a mean strength of ~ 280 MPa in biaxial flexure, was produced by ion-exchange in molten sodium nitrate.

1. Introduction

Much effort has been devoted to the determination of the structure of a whole range of borate-based glasses, for example, [1–7]. Until relatively recently, however, little interest has been shown in the potential applications for these materials, with the exception of their use as relatively low-temperature sealing media, that is, as solder glasses [8, 9]. Currently, renewed interest is being shown in borate-based glasses, particularly in the alkali borates, because of their potential as fast ionic conductors for use in solid-state lithium batteries and related applications [6, 10–13], and in radiation and thermoluminescence dosimetry devices [14]. Unfortunately, as a class of material, borate glasses suffer from several serious disadvantages in comparison to conventional silicate systems. For example, they possess lower mechanical strength, than silicate glasses and, in addition, they exhibit very poor chemical durability, being readily attacked on exposure to atmospheric moisture. It is therefore desirable that a range of techniques is examined in order that suitable methods can be identified for improving the overall properties of borate glasses.

2. Methods for improving the properties of glasses

2.1. Mechanical properties

In principle, there are a number of routes by which the mechanical properties of oxide glasses can be improved, although these methods have generally only been applied to silicate glasses [15]. These routes can be divided into bulk or surface methods and they include the use of bulk crystallization to produce a polycrystalline glass–ceramic material, the use of surface crystallization or chemical ion-exchange to provide a surface compressive layer, and the use of fibre reinforcement to produce a composite material. It is also possible, in principle, to increase the strength of glasses very significantly simply by removing surface flaws.

2.1.1. Bulk methods

2.1.1.1. The use of bulk crystallization to produce a glass–ceramic. The success of a glass–ceramic process in terms of producing mechanically strong, fine-grained polycrystalline ceramic materials is strongly dependent on inducing a high crystal nucleation density within the glass by providing a very large number of internal heterogeneities from which the major crystalline phases can form and grow. This can be achieved in practice by the use of specific nucleating agents, which are added to the glass batch (for example, see [6, 17]). Nucleating agents act either by inducing the glass to phase separate on a very fine scale, or by forming small crystallites (which may be composed of the nucleating phase itself or of some compound formed by reaction with the constituents in the glass). In either case, many small heterogeneities are produced, onto which the major crystalline phases can nucleate and grow. Although a large amount of information is available on the controlled bulk crystallization of silicate glasses [15], only very limited work has been reported on the crystallization behaviour of borate glasses [18–23] and, in general, the crystallization of these materials proceeds from the surface rather than internally. The resultant mechanical properties of crystalline and partially crystalline borate materials have not been recorded, but they are expected to be poor due to the deleterious influence of uncontrolled surface crystallization.

A number of additions may be suitable as nucleating agents for lithium borate systems, including P_2O_5 or LiF, which may promote phase separation, and MoO_3, which (under suitable conditions) may react with Li_2O to form Li_2MoO_4 nuclei. A list of potential nucleating agents, together with the corresponding most likely nucleation mechanism for borate glasses, is given in Table I.

2.1.1.2. Fibre reinforcement. The use of high elastic-modulus fibres, for example, carbon or silicon carbide,

0022–2461

TABLE I Potential nucleating agents for the controlled crystallization of lithium borate glass

Potential nucleating agent	Proposed mechanism
P_2O_5	Phase separation
LiF	Phase separation
TiO_2	Phase separation or $TiO_2 + Li_2O \rightarrow Li_2TiO_3$ crystallites
MoO_3	Phase separation or $MoO_3 + Li_2O \rightarrow Li_2MoO_4$ crystallites
WO_3	Phase separation or $WO_3 + Li_2O \rightarrow Li_2WO_4$ crystallites
Bi_2O_3	Phase separation or $Bi_2O_3 + Li_2O \rightarrow Li_2Bi_2O_4$ crystallites
V_2O_5	Phase separation or precipitation of V_2O_5 crystallites
ZnO	Phase separation or precipitation of ZnO crystallites
CuO	Production of metallic Cu crystallites
Sb_2O_3	Phase separation

in a lower modulus matrix is a well-known and routinely practised technique for improving the strength of materials, including inorganic glasses (see for example, [15]). Fibre reinforcement can also be employed to increase substantially the work of fracture and fracture toughness of such materials, and to prevent the catastrophic-failure mode which is associated with brittle materials.

2.1.2. Surface methods

2.1.2.1. Removal of surface flaws. Since failure of a brittle material is almost invariably initiated from the surface due to the presence of small flaws, a considerable improvement in the strength can be achieved by removing these flaws. This can be achieved in practice by mechanical or chemical means, for example, by polishing or etching. Unfortunately, the strength improvements obtained in this manner are only temporary, unless steps are taken to protect the surface by the provision of a suitable abrasion-resistant and compatible coating.

2.1.2.2. Production of a surface compressive layer. A number of methods have been devised for generating surface compressive layers [15]. These include thermal strengthening (also known as *thermal toughening* or *tempering*) and chemical ion-exchange strengthening, in addition to controlled surface crystallization or cladding to provide a surface layer with a lower thermal expansion than that of the bulk glass. Strength increases are achieved because the compressive stress at the surface must be overcome before defects are subjected to tensile forces. As a rough guide, the strength of a glass article with a surface compressive stress is equal to the magnitude of the compressive stress plus the normal fracture strength of the untreated material. In order to impart a useful strength, the depth of the compressive layer must generally be greater than the size of typical flaws, that is greater than 50 μm. Although these methods have generally been applied to silicate systems only, it may be feasible to use such techniques for improving the properties of borate glasses.

2.2. Chemical durability

A major concern in many potential applications is the very poor chemical durability of borate glasses, particularly their highly hygroscopic behaviour. In general, the durability may be improved by compositional modification; alternatively, a durable barrier coating may be employed.

3. Experimental procedures

3.1. Preparation of glass samples

Lithium borate based materials with the general composition $Li_2O \cdot xB_2O_3$ were prepared with x in the range 2.0–5.0 using lithium carbonate and boric acid as the starting materials. The batch materials were dried at 100 °C for a minimum of 3 h before weighing out appropriate amounts of powder, calculated to yield 100 g of glass, and mixing by tumbling for 1 h in a polyethylene bottle. The mixed batch was then calcined at 450–500 °C for 1 h in an alumina crucible. More recent work has shown that the initial calcining stage can be dispensed with by using fused B_2O_3 as a replacement for boric acid. The glass batch was subsequently melted at 1000–1100 °C in a Pt–5%Rh crucible fitted with a lid. The melt was then cast onto a stainless-steel plate at room temperature to give a material of variable thickness. Subsequently, a qualitative assessment of the glass-forming ability (GFA) of the material was made from a knowledge of the maximum thickness of the material that could be vitrified. A number of ternary glasses were also prepared, with the general composition $Li_2O \cdot xB_2O_3 + 5$ wt%SiO_2, in addition to a number of quaternary compositions, that is, $Li_2O \cdot xB_2O_3 + 5$ wt%$SiO_2 + 2$ or 5 wt% Al_2O_3 or MgO. On the basis of this work, the compositions $Li_2O \cdot xB_2O_3 + 5$ wt%SiO_2, for $x = 3.0$ and 3.5, were selected for more detailed investigation, and 1 kg batches of these glasses were prepared, using the same procedure as was used in the preparation of the smaller batches. Subsequently, further 100 g samples of glass were prepared in order to assess the effect of a number of additional additives on the properties, particularly the nucleating efficiency and the durability of the two compositions chosen for more detailed study. The compositions which were investigated are summarized in Table II.

Bulk samples were prepared by casting molten glass into preheated (to 450 °C) graphite moulds with diameters of 38 mm to give solid cylinders of glass which were ~ 80 mm in height. These cylinders were immediately annealed for 1 h and then they were furnace cooled to room temperature at ~ 0.5 °C min^{-1}. Disc samples ~ 1.5 mm thick were subsequently cut from the cylinders using a diamond wheel. Before further treatment, the discs were cleaned using water-free methanol.

TABLE II Borate glass compositions

Glass code	Composition
LB1	$Li_2O \cdot 2B_2O_3$
LB3	$Li_2O \cdot 2.5B_2O_3$
LB4	$Li_2O \cdot 2.75B_2O_3$
LB5	$Li_2O \cdot 3B_2O_3$
LB8	$Li_2O \cdot 3.5B_2O_3$
LB15	$Li_2O \cdot 4B_2O_3$
LB18	$Li_2O \cdot 4.5B_2O_3$
LB20	$Li_2O \cdot 5B_2O_3$
LB2	$Li_2O \cdot 2B_2O_3$ + 5wt%SiO_2
LB6	$Li_2O \cdot 3B_2O_3$ + 5wt%SiO_2
LB9	$Li_2O \cdot 3.5B_2O_3$ + 5wt%SiO_2
LB16	$Li_2O \cdot 4B_2O_3$ + 5wt%SiO_2
LB19	$Li_2O \cdot 4.5B_2O_3$ + 5wt%SiO_2
LB21	$Li_2O \cdot 5B_2O_3$ + 5wt%SiO_2
LB12	$Li_2O \cdot 3.5B_2O_3$ + 5wt%SiO_2 + 2wt %MgO
LB10	$Li_2O \cdot 3.5B_2O_3$ + 5wt%SiO_2 + 2wt %Al_2O_3
LB14	$Li_2O \cdot 3.5B_2O_3$ + 5wt%SiO_2 + 2wt %P_2O_5
LB13	$Li_2O \cdot 3.5B_2O_3$ + 5wt%SiO_2 + 5wt %MgO
LB7	$Li_2O \cdot 3B_2O_3$ + 5wt%SiO_2 + 5wt %Al_2O_3
LB11	$Li_2O \cdot 3.5B_2O_3$ + 5wt%SiO_2 + 5wt %Al_2O_3
LB17	$Li_2O \cdot 4B_2O_3$ + 5wt%SiO_2 + 5wt %Al_2O_3
LB6A	$Li_2O \cdot 3B_2O_3$ + 5wt%SiO_2 + 1mol %P_2O_5
LB6B	$Li_2O \cdot 3B_2O_3$ + 5wt%SiO_2 + 2mol %P_2O_5
LB6C	$Li_2O \cdot 3B_2O_3$ + 5wt%SiO_2 + 2mol %LiF
LB6D	$Li_2O \cdot 3B_2O_3$ + 5wt%SiO_2 + 3mol %LiF
LB6E	$Li_2O \cdot 3B_2O_3$ + 5wt%SiO_2 + 0.5mol %ZnO
LB6F	$Li_2O \cdot 3B_2O_3$ + 5wt%SiO_2 + 1.0mol %ZnO
LB6G	$Li_2O \cdot 3B_2O_3$ + 5wt%SiO_2 + 2mol %Sb_2O_3
LB9A	$Li_2O \cdot 3.5B_2O_3$ + 5wt%SiO_2 + 1.5mol %P_2O_5
LB9B	$Li_2O \cdot 3.5B_2O_3$ + 5wt%SiO_2 + 1.5mol %MoO_3
LB9C	$Li_2O \cdot 3.5B_2O_3$ + 5wt%SiO_2 + 1.5mol %WO_3
LB9D	$Li_2O \cdot 3.5B_2O_3$ + 5wt%SiO_2 + 1.5mol %V_2O_5
LB9E	$Li_2O \cdot 3.5B_2O_3$ + 5wt%SiO_2 + 1mol %ZnO
LB9G	$Li_2O \cdot 3.5B_2O_3$ + 5wt%SiO_2 + 1.5mol %CuO
LB9H	$Li_2O \cdot 3.5B_2O_3$ + 5wt%SiO_2 + 1.5mol %Bi_2O_3
LB9I	$Li_2O \cdot 3.5B_2O_3$ + 5wt%SiO_2 + 1.5mol %TiO_2
LB9J	$Li_2O \cdot 3.5B_2O_3$ + 5wt%SiO_2 + 1.5mol %LiF

3.2. Measurement of the thermal properties

The characteristic temperatures of the glasses in the form of a crushed as-cast powder with a particle size of 0.6–1.0 mm were monitored using a Stanton Redcroft Model 674 differential thermal analyser. The differential thermal analyser (DTA) was calibrated over a range of temperatures using standard materials (for example K_2SO_4 and Ag_2SO_4). A heating rate of 10 °C min^{-1} was used in all the investigations. The temperatures measured included the glass-transition temperature, T_g, together with the temperatures corresponding to the crystallization peaks, T_{xp_1}, T_{xp_2} etc., and the liquidus, or end of melting temperature, T_{liq}. A minimum of three samples were measured for each determination.

A preliminary assessment of the effect of a number of additives on the ability to act as crystal-nucleating agents for the borate glasses was made using the method of Thakur and Thiagarajan [24]. In this method, the variation in the peak crystallization temperature with the particle size was monitored. Two particle-size fractions were used in our experiments, 0.6–1.0 mm and less than or equal to 212 μm. In general, the greater than the difference in crystallization temperature that is noted between the coarse and the fine glass samples, the less efficient is the bulk crystallization, that is, surface crystallization predominates. An attempt was then made to define an optimum nucleating temperature for a number of systems using the method of Marotta *et al.* [25–28]. In this technique, the optimum nucleating temperature is found by plotting the difference in the crystallization peak temperatures of as-quenched and nucleated glass samples ($\Delta T_{Marotta} = T_p^0 - T_{p_{nuc}}$) against the temperature of nucleation, T_{nuc}. If bulk crystallization is effective, a maximum is obtained when $\Delta T_{Marotta}$ is plotted against T_{nuc}. In the present work, glass samples with particles size of 0.6–1.0 mm were nucleated *in situ* in the DTA for 1 h at temperatures in the range 500–620 °C. The peak crystallization temperatures were then monitored by heating the samples through the crystallization range.

3.3. Assessment of the glass-forming ability and of the thermal stability

A preliminary qualitative assessment of the glass-forming ability (GFA) of the glasses was made on the basis of the maximum thickness of (crystal-free) glass that could be produced by pouring the melt onto a stainless steel plate. A good GFA was defined in the present work for those materials which were capable of forming a glass which was totally free from areas of visible crystallinity in a thickness greater than 10 mm upon pouring the material onto the metal plate. A semiquantitative assessment of the GFA of a material is also possible using the thermal parameter T_g/T_{liq} (called the *reduced glass temperature*), which is related to the critical cooling rate for glass formation, T_{crit} [29]. For a given class of material which exhibit approximately similar melt viscosities, the higher is the value of the reduced glass temperature the lower is T_{crit}, and the higher is the GFA (and the greater is the thickness of glass that can be produced), as illustrated in Fig. 1.

The *thermal stability* of the resulting glass is of additional practical importance. The stability must be high enough to enable the glass to be worked using conventional glass-forming routes (that is, pressing, blowing etc., followed by annealing) without the occurrence of uncontrolled devitrification of the glass (which would alter the temperature–viscosity characteristics of the glass and which would result in a loss of control over the working processes). The thermal stability can be related to the working range of the glass, which is the temperature interval between T_g and some function of crystallization ($\Delta T_{WR} = T_X - T_g$). The smaller this temperature interval is, the lower is the thermal stability of the glass, and the more difficult it is to avoid partial crystallization during working or annealing operations, or even during cooling of the melt.

3.4. Assessment of the chemical durability

The chemical durability of glasses was qualitatively assessed by examining samples after exposure, for

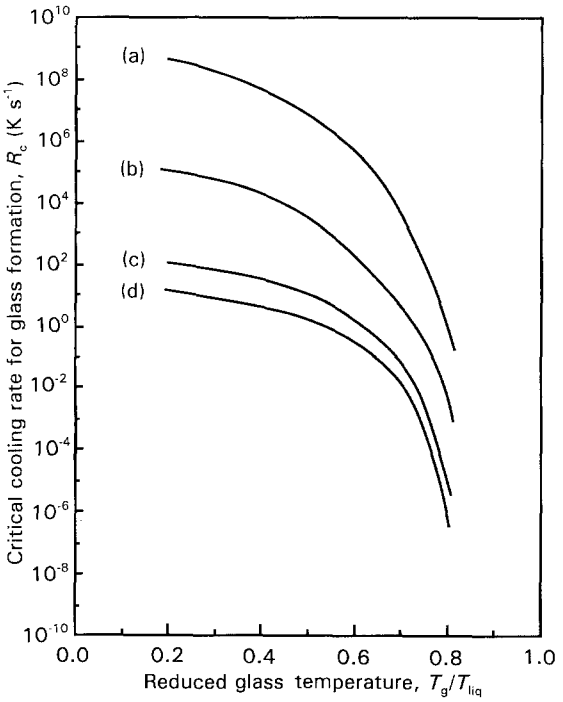

Figure 1 The critical cooling rate for glass formation, R_c, as a function of the reduced glass temperature, T_g/T_{liq}, for different melt viscosities: (a) 10^{-2} Pa s, (b) 10 Pa s, (c) 10^4 Pa s, and (d) 10^6 Pa s.

various periods of time, to a laboratory atmosphere. The most promising compositions were then subjected to a more rigorous quantitative assessment using a purpose-built durability rig [30] in which glass discs were held in perspex cells containing deionized water at a given temperature, the water being continuously stirred. The discs were weighed before and after exposure.

3.5. Thermal-expansion characteristics

The thermal expansion of selected rod samples was measured in air using a dilatometer (Ceramic Developments (Midlands) Ltd. UK) operating at a heating rate of 5 °C min^{-1}, over the temperature range 20–450 °C.

3.6. X-ray diffraction

As-cast and heat-treated samples were examined using a Philips PW 1710 diffractometer employing CuK_α radiation over the range $2\theta = 5$–100°.

3.7. Microstructures

The microstructures were examined by optical microscopy, after the mounting and polishing of the samples. The fracture surfaces and the treated surfaces were examined using scanning electron microscopy (SEM). Samples for SEM were coated with an Au–Pd alloy prior to examination with a Cambridge S360 scanning electron microscope.

3.8. Strengthening methods

3.8.1. Bulk methods

3.8.1.1. Bulk crystallization. Glass cylinders measuring 38 mm in diameter by ~ 10 mm high were cleaned in methanol in order to remove all the surface contaminants, which may give rise to preferential surface crystallization, and they were then subjected to a range of heat-treatment schedules in air. The heating schedules employed were derived from the DTA data which are reported in Section 4.1. The heating rates were maintained at ~ 5 °C min^{-1} during this process, while cooling rates were kept to ~ 0.5 °C min^{-1}.

3.8.1.2. Fibre reinforcement. A number of composite samples containing ~ 40 vol.% carbon-fibre reinforcement were prepared for us by AEA(T) technology. The samples were produced by infiltration of carbon-fibre tows by glass-powder slurries based on methyl ethyl ketone with a poly(vinyl acetate) binder. The impregnated tows were subsequently dried, cut into strips 50 × 15 mm in size, laid up in stacks of six in a graphite mould, and then hot pressed at a pressure of 7 MPa and a temperature of 700 °C for 20 min under argon. The pressing schedule which was employed is illustrated graphically in Fig. 2.

3.8.2. Surface modification

3.8.2.1. Etching. Disc samples were etched for 2 min in an aqueous solution of 9%HF + 7%H_2SO_4, and they were then cleaned in methanol and dried using an infrared lamp. Some samples were also etched using pure deionized water.

3.8.2.2. Chemical ion-exchange. Etched and dried disc samples were weighed to an accuracy of 0.0001 g and then they were treated with molten sodium or potassium nitrate contained in a 1 l capacity stainless-steel beaker for various lengths of time at a standard temperature of 385 °C. The weight change per

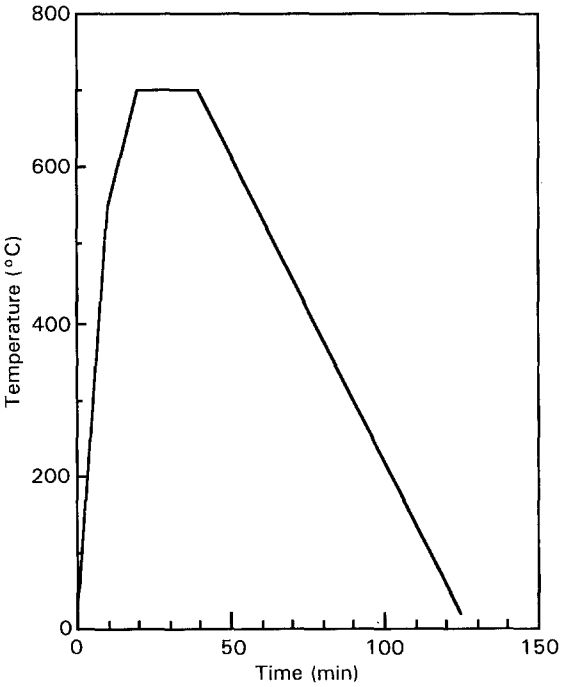

Figure 2 A hot-pressing schedule for the preparation of carbon-fibre-reinforced lithium borate glass composites.

unit area for each disc sample was derived by weighing and by micrometric measurements. An attempt was then made to measure the stress profiles of the treated samples using the scattered light and etching method developed at AWE, as described previously for silicate glasses [30–33].

3.9. Mechanical-property measurements

3.9.1. Biaxial flexure strength

The mechanical properties of the disc samples (with a 38 mm diameter and a 1.4 mm thickness) were monitored in biaxial flexure employing the piston-on-three-ball method [34–37]. In this technique, a glass sample in the form of a thin disc is supported on three equally spaced ball bearings situated on a circle of diameter d, and a piston is used to transmit the load to the central region of the disc. In the present work, the 38 mm diameter discs were tested using a piston with a diameter of 2.4 mm, and with $d = 25.4$ mm. A constant loading rate of 0.75 mm min^{-1} was used. The biaxial flexure strength, σ_{biax}, was calculated using the relationship

$$\sigma_{biax} = \frac{3P(1+\nu)}{4\pi t^2}\left(1 + 2\ln\frac{a}{b} + \frac{1-\nu}{1+\nu}\right)\left(\frac{1-b^2}{2a^2}\right)\frac{a^2}{R^2} \quad (1)$$

where P is the load at fracture, ν is the Poisson's ratio for the glass (a standard value of 0.24 was taken for all materials investigated), t is the sample thickness, a is the radius of the support points, b is the radius of the piston and R is the radius of the sample (for the testing rig employed, $a = 12.70$ mm and $b = 1.19$ mm). A minimum of ten samples was used for each determination.

This particular technique offers the advantage that the fracture stress is relatively insensitive to the condition of the edges of the sample. It is therefore possible, in principle, to resolve intrinsic trends in the strength data.

3.9.2. Three-point bending

The mechanical properties of the carbon-fibre-reinforced composite bars (measuring $\sim 50 \times 5 \times 1.5$ mm) were monitored in three-point bending using a span of 40 mm and a cross-head speed of 0.5 mm min^{-1}. Bending strength, σ_{bend} and the Young's modulus, E, were calculated using standard expressions. A minimum of ten samples was employed for each determination.

The work-of-fracture values were calculated by integration of the area under the load–deflection curves; an arbitrary limit of 2.5 times the displacement at the peak stress was taken as the limit of useful work of fracture.

3.9.3. Microhardness measurements

The microhardness of selected glasses was measured with a Matsuzawa model DMH-1 microhardness tester. A standard load of 200 g and a loading time of 15 s was used. A minimum of ten readings was taken for each measurement.

4. Results

4.1. Thermal investigations

Thermal data for the glasses are reported in Table III. Representative DTA traces are shown in Fig. 3. In general, well-defined glass transitions, crystallization peaks and melting ranges were observed. Characteristic temperatures as a function of the glass composition are given in Figs. 4–7. In Fig. 4a, T_g decreases as the B_2O_3 content increases. More complex behaviour is observed with crystallization (Figs 4b–6). In all cases, addition of 5 wt% SiO_2 increased the characteristic temperatures. Nucleating efficiencies, as determined by the variation in the peak crystallization temperatures between coarse and fine samples of glass, are given in Table IV. Data for determining optimum nucleating temperatures (Marotta plots) are shown in Fig. 8, where it may be noted that discrete maxima were not obtained. A thermal-expansion trace for one of the samples (LB6) is given in Fig. 9. This glass had a thermal-expansion coefficient of $8.0 \times 10^{-6}\,°C^{-1}$ over the temperature range 20–450 °C.

4.2. The glass-forming ability and the thermal stability

Binary lithium-borate glasses have been successfully prepared as bulk samples several millimetres thick containing up to ~ 29 mol % Li_2O. The Li_2O content can be increased to ~ 33 mol % by incorporation of 5 wt % SiO_2. Qualitative data for the GFA of a range of materials are given in Table V, whilst semiquantitative GFA data, (T_g/T_{liq}) are given in Table III and Fig. 10. Thermal-stability data (working ranges) are given in Fig. 11. In all cases addition of 5 wt % SiO_2 increased the working range.

4.3. Chemical durability

Qualitative data for the chemical durability of glasses are summarized in Table V. Quantitative durability data for a selected sample are given in Table VI and in Fig. 12.

4.4. Mechanical properties

The biaxial flexure strength of as-machined lithium borate glass discs was 75 ± 13 MPa. This is lower than typical silicate glasses, which have averages around 100 MPa.

4.4.1. Strengthening methods

4.4.1.1. Bulk crystallization. Details of the samples and of the heat-treatment schedules which were employed, together with the phases produced, are given in Table VII. Glass LB6 ($Li_2O \cdot 3B_2O_3$ + 5 wt % SiO_2) underwent partial melting during the heat-treatment schedule to form a liquid phase which exuded from the

TABLE III Thermal properties of lithium-borate-based glasses

Glass code	T_g (°C)	$T_{xp_{1a}}$ (°C)	$T_{xp_{1m}}$ (°C)	T_{xp_1} (°C)	T_{xp_2} (°C)	T_{liq} (°C)	ΔT_{WR} (°C)	T_g/T_{liq} ($K K^{-1}$)
LB3	513 ± 1	545 ± 19	573 ± 17	591 ± 19	660 ± 19	910 ± 6	60	0.664
LB4	512 ± 4	557 ± 14	581 ± 5	588 ± 4	633 ± 5	893 ± 4	69	0.673
LB5	510 ± 6	574 ± 7	583 ± 7	589 ± 8	699 ± 1	872 ± 2	73	0.684
LB8	506 ± 9	548 ± 4	569 ± 8	579 ± 2	–	846 ± 6	63	0.696
LB15	496 ± 1	547 ± 2	571 ± 0	587 ± 2	801 ± 0	836 ± 2	75	0.693
LB18	483 ± 6	558 ± 2	577 ± 1	610 ± 2	–	830 ± 2	94	0.685
LB20	457 ± 1	562 ± 3	575 ± 3	606 ± 1	–	771 ± 1	118	0.699
LB2	509 ± 0	598 ± 2	610 ± 2	638 ± 1	–	908 ± 1	101	0.662
LB6	514 ± 4	633 ± 3	660 ± 3	690 ± 4	774 ± 1	871 ± 1	146	0.688
LB9	503 ± 3	632 ± 7	655 ± 9	684 ± 8	779 ± 6	833 ± 2	152	0.702
LB16	493 ± 1	628 ± 4	641 ± 6	682 ± 6	–	825 ± 1	148	0.698
LB19	486 ± 0	631 ± 1	642 ± 1	699 ± 2	–	781 ± 2	156	0.720
LB21	458 ± 6	604 ± 5	611 ± 5	666 ± 5	–	761 ± 4	153	0.707
LB12	510 ± 2	646 ± 1	672 ± 2	717 ± 1	–	832 ± 1	162	0.709
LB10	504 ± 2	634 ± 1	650 ± 6	716 ± 2	–	843 ± 4	146	0.696
LB14	498 ± 2	630 ± 3	652 ± 3	706 ± 5	–	822 ± 1	154	0.704
LB13	498 ± 1	630 ± 1	644 ± 7	727 ± 2	–	833 ± 1	146	0.697
LB7	506 ± 1	638 ± 1	660 ± 3	722 ± 2	–	851 ± 1	154	0.693
LB11	496 ± 3	636 ± 3	645 ± 2	738 ± 0	–	832 ± 0	149	0.696
LB17	482 ± 4	620 ± 0	638 ± 0	679 ± 4	–	–	156	–
LB6A	507 ± 2	629 ± 2	660 ± 4	699 ± 8	773 ± 5	846 ± 2	153	0.697
LB6B	502 ± 2	629 ± 2	656 ± 6	715 ± 3	742 ± 2	823 ± 3	154	0.707
LB6C	505 ± 2	627 ± 1	663 ± 2	695 ± 1	755 ± 2	868 ± 2	158	0.682
LB6D	502 ± 1	625 ± 2	661 ± 2	690 ± 2	726 ± 4	872 ± 3	159	0.677
LB6E	510 ± 1	631 ± 1	664 ± 5	697 ± 2	771 ± 1	868 ± 2	154	0.686
LB6F	506 ± 3	628 ± 1	656 ± 3	699 ± 4	774 ± 2	864 ± 2	150	0.685
LB6G	496 ± 4	–	674 ± 4	702 ± 4	754 ± 4	852 ± 4	178	0.684
LB9A	491 ± 1	625 ± 2	648 ± 5	705 ± 2	775 ± 1	817 ± 3	157	0.701
LB9B	495 ± 2	627 ± 2	652 ± 2	694 ± 2	–	779 ± 2	157	0.701
LB9C	498 ± 2	623 ± 2	639 ± 2	679 ± 2	759 ± 2	822 ± 2	141	0.704
LB9D	482 ± 2	607 ± 2	625 ± 2	681 ± 2	–	747 ± 2	143	0.740
LB9E	503 ± 2	623 ± 2	657 ± 2	699 ± 2	780 ± 2	826 ± 2	154	0.706
LB9G	504 ± 2	632 ± 2	665 ± 2	700 ± 2	774 ± 2	835 ± 2	161	0.701
LB9H	498 ± 2	623 ± 2	654 ± 2	690 ± 2	768 ± 2	835 ± 2	156	0.696
LB9J	505 ± 2	633 ± 2	659 ± 2	691 ± 2	774 ± 2	838 ± 2	154	0.700

T_g = glass-transition temperature (midpoint).
$\Delta T_{WR} = (T_{xp_{1a}} - T_g)$.
T_g/T_{liq} = reduced glass temperature.

sample. This effect was suppressed for a similar glass by an addition of P_2O_5. In both cases, a white crystalline product was formed; however, these products were mechanically weak and friable in nature.

4.4.1.2. Fibre reinforcement. The microstructure of a sectioned and polished carbon-fibre reinforced glass samples is shown in Fig. 13. Fig. 13 shows that the distribution of the carbon fibres was not uniform; regions of glass which are denuded of carbon fibres are apparent. Some matrix porosity is also visible. A mean strength of 144 MPa together with a work of fracture of 4.2 kJ m^{-2} was obtained. The fracture surfaces shown in Fig. 14 illustrate the non-catastrophic failure mode.

4.4.1.3. Etching. Micrographs of sample surfaces subjected to machining, and etching in aqueous HF and pure water are shown in Fig. 15. It may be noted that the samples etched in HF were quite different in appearance to those etched in pure water, with the water-etched samples exhibiting smooth bubble-like surface features. The etched samples had a reasonable mechanical strength (that is ~ 155 MPa), but these values were reduced by light abrasion with 120 grit SiC paper.

4.4.1.4. Chemical ion-exchange. Micrographs of the surfaces of samples that have undergone chemical ion-exchange are shown in Fig. 16. These surfaces exhibit pitted regions, although it may be noted that the profile of the scratch which is visible in Fig. 16b is quite smooth, suggesting that the treatment is effective at removing the sharp edges of defects. The mechanical properties (the biaxial flexure strength and the microhardness) are summarized in Table VIII and Figs 17 and 18. A value of 282 MPa was noted for the mean strength of the strongest material; however, the high-strength values were again reduced by light abrasion.

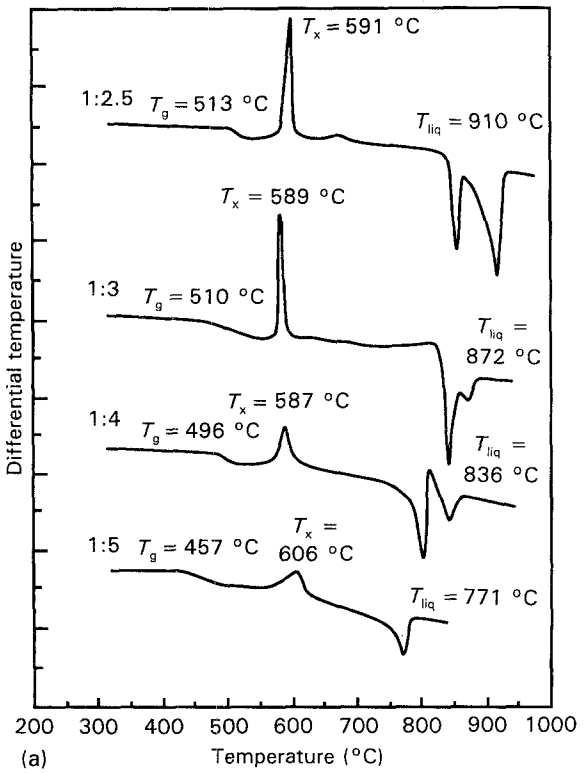

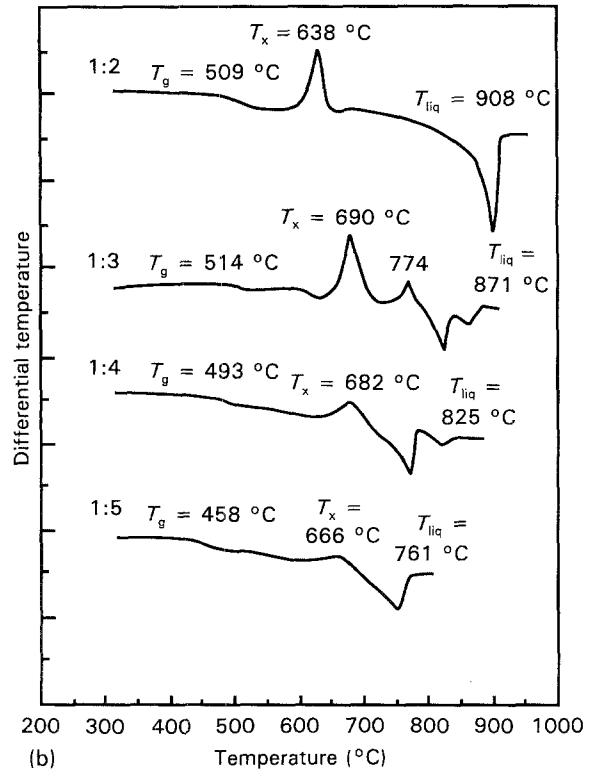

Figure 3 Typical DTA traces of a number of borate glasses: (a) binary $Li_2O \cdot xB_2O_3$ glass, and (b) ternary $Li_2O \cdot xB_2O_3$ + 5wt % SiO_2 glass.

4.5. X-ray data

X-ray data for some samples are summarized in Table VII and Fig. 19. The major phases were LiB_3O_5 and $Li_2B_4O_7$, and there was some residual glass. A greater proportion of $Li_2B_4O_7$ and the residual glass was found in the sample containing P_2O_5.

5. Discussion

5.1. Characteristic thermal data

The overall trend that T_g decreased as the B_2O_3 content increased which was noted for the binary lithium borate glasses, as shown in Fig. 4a, has been observed previously (for example, in [38, 39]) and it has been attributed to a decrease in the number of tetrahedral borate units as the B_2O_3 content increases.

5.2. Glass-forming ability and thermal stability of lithium borate glasses

From a practical point of view, a glass-forming material must possess a sufficiently high GFA *and* a suffi-

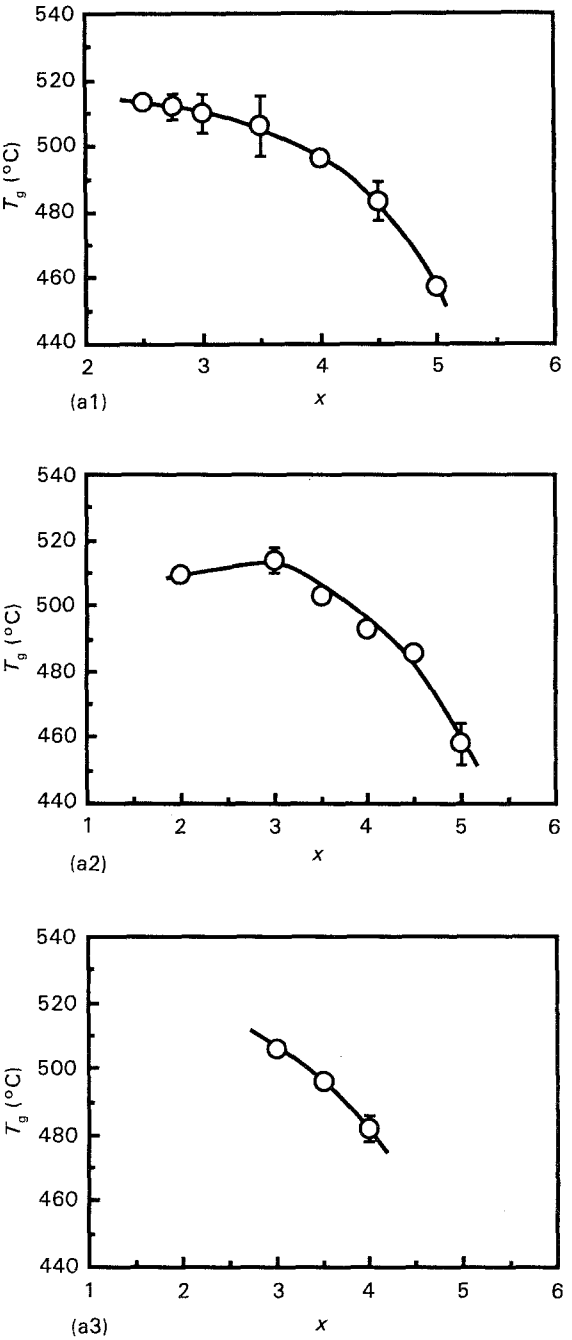

Figure 4 Characteristic temperatures of borate glasses as a function of the composition: (a) T_g for all the glasses, (a1) $Li_2O \cdot xB_2O_3$; (a2) $Li_2O \cdot xB_2O_3$ + 5wt %SiO_2; (a3) $Li_2O \cdot xB_2O_3$ + 5wt %SiO_2 + 5wt %Al_2O_3. (b) crystallization-temperature data (peak start, extrapolated peak start, and peak crystallization temperatures) for $Li_2O \cdot xB_2O_3$ glasses, and (c) crystallization-temperature data for $Li_2O \cdot xB_2O_3$ + 5wt %SiO_2 compositions.

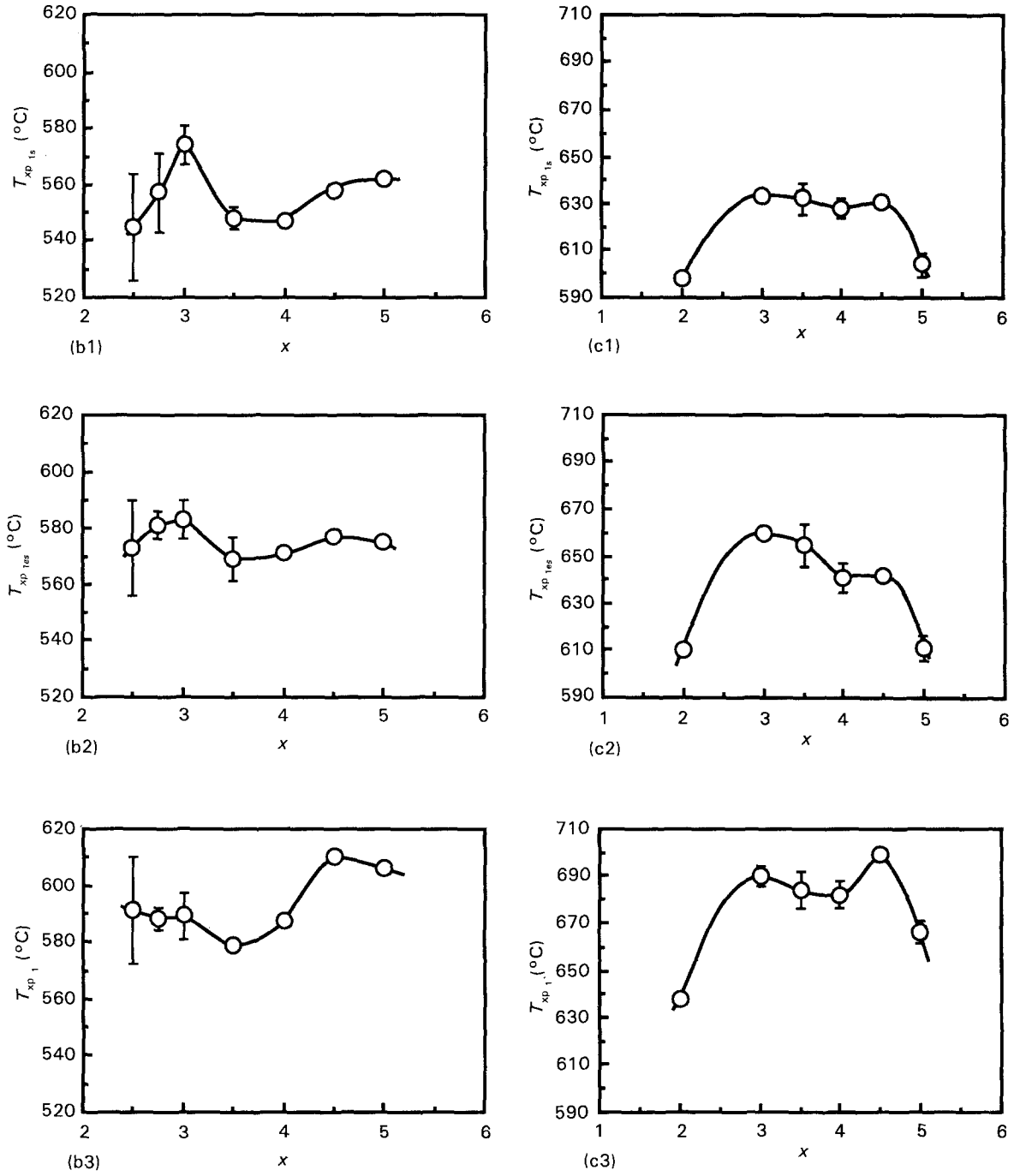

Figure 4 (continued).

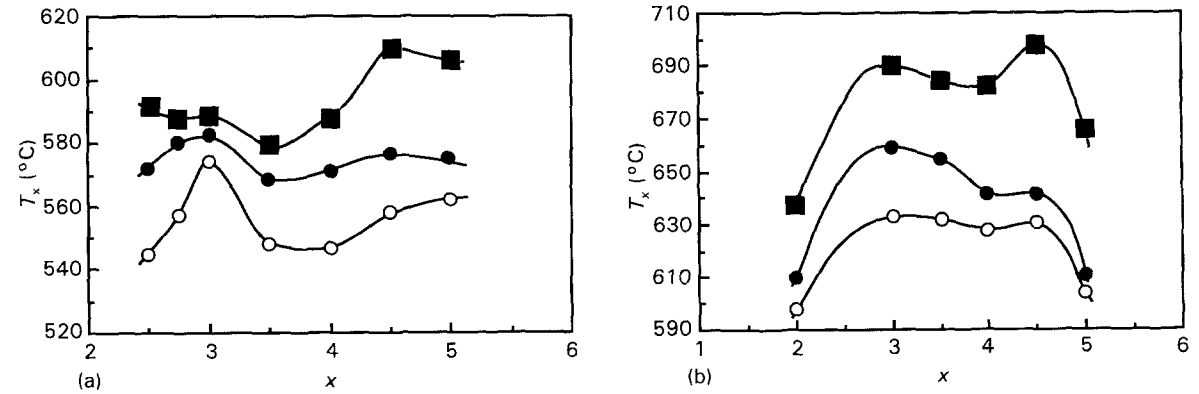

Figure 5 A summary of the crystallization-temperature data: (○) peak start, (●) extrapolated peak start, and (■) peak (a) $Li_2O \cdot xB_2O_3$, and (b) $Li_2O \cdot xB_2O_3$ + 5wt %SiO_2.

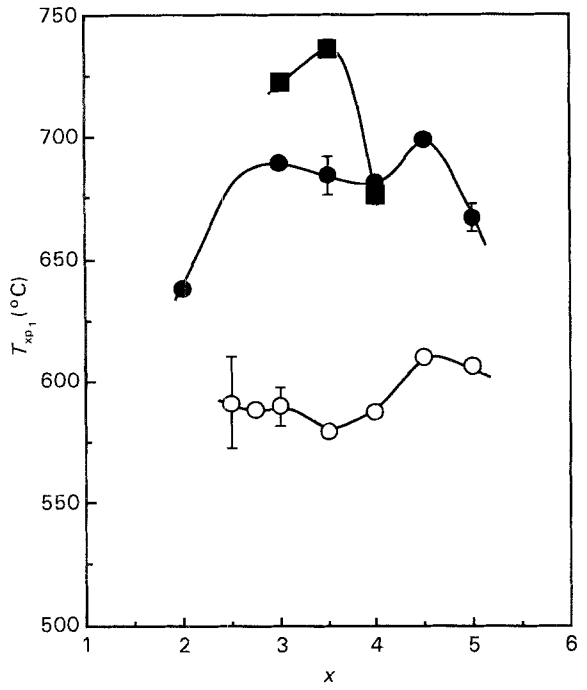

Figure 6 Summary of the peak crystallization temperature data for: (○) $Li_2O \cdot xB_2O_3$, (●) $Li_2O \cdot xB_2O_3$ + 5wt %SiO_2, and (■) $Li_2O \cdot xB_2O_3$ + 5wt %SiO_2 + 5wt %Al_2O_3.

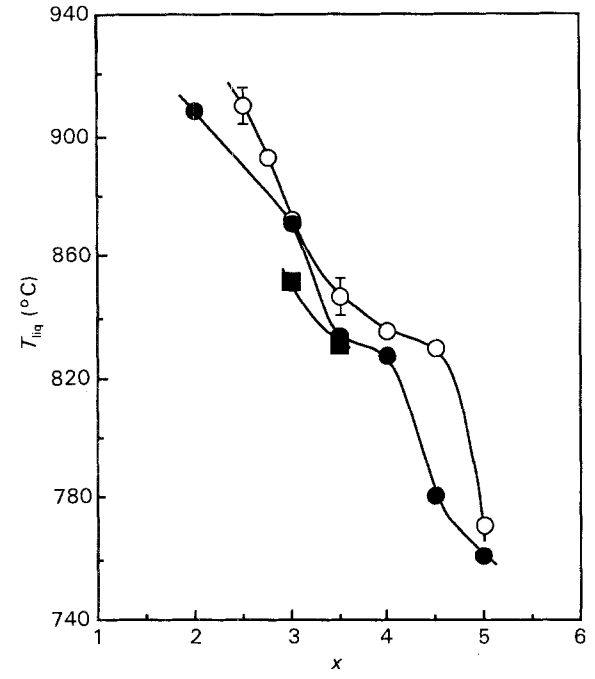

Figure 7 A summary of liquidus-temperature data for all the glasses. (For key, see Fig. 6.)

ciently long working range commensurate with the proposed application, i.e., dependent on the thickness of glass required and the temperature (and time) of any working or annealing operations required. The phase diagram for the binary Li_2O–B_2O_3 system is shown in Fig. 20 [40]. The glass-forming range, as determined in the present investigation for 100 g batches of glass poured onto a stainless-steel plate to give a solidified melt greater than 4–5 mm thick, extends from B_2O_3 to beyond the $2Li_2O \cdot 5B_2O_3$ bound-

TABLE IV The effect of small concentrations of additives on the nucleating efficiency

Glass code	Additive	Concentration (mol %)	ΔT_{xp_1} (°C)	ΔT_{xp_2} (°C)
LB6	None	0.0	33	4
LB6G	Sb_2O_3	2.0	21	20
LB9	None	0.0	33	4
LB9A	P_2O_5	1.5	24	5
LB9B	MoO_3	1.5	37	–
LB9C	WO_3	1.5	32	2
LB9D	V_2O_5	1.5	51	–
LB9E	ZnO	1.5	28	20
LB9G	CuO	1.5	27	4
LB9H	Bi_2O_3	1.5	22	2
LB9J	LiF	1.5	26	19

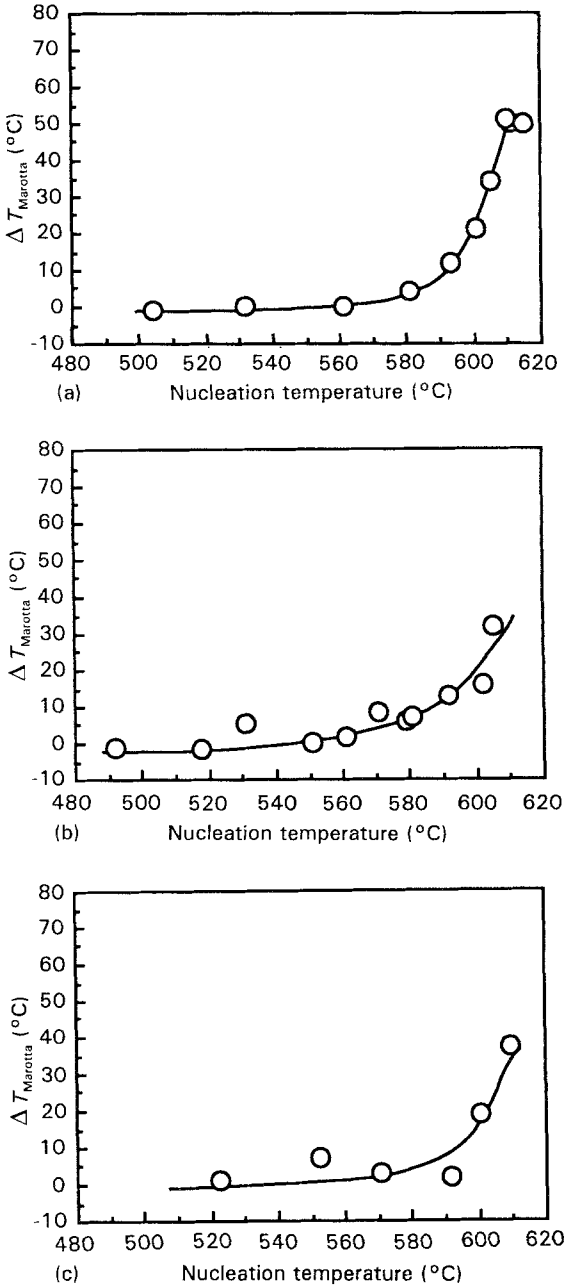

Figure 8 The variation in the peak crystallization temperature, $\Delta T_{Marotta}$, between the as-quenched and nucleated $Li_2O \cdot 3B_2O_3$ + 5wt %SiO_2, glasses as a function of the temperature of nucleation (Marotta plots). Plots are shown for a variety of additives (see text for details): (a) no additive; (b) 1 mol % P_2O_5, (c) 2 mol % P_2O_5, (d) 3 mol % LiF, and (e) 0.5 mol % ZnO.

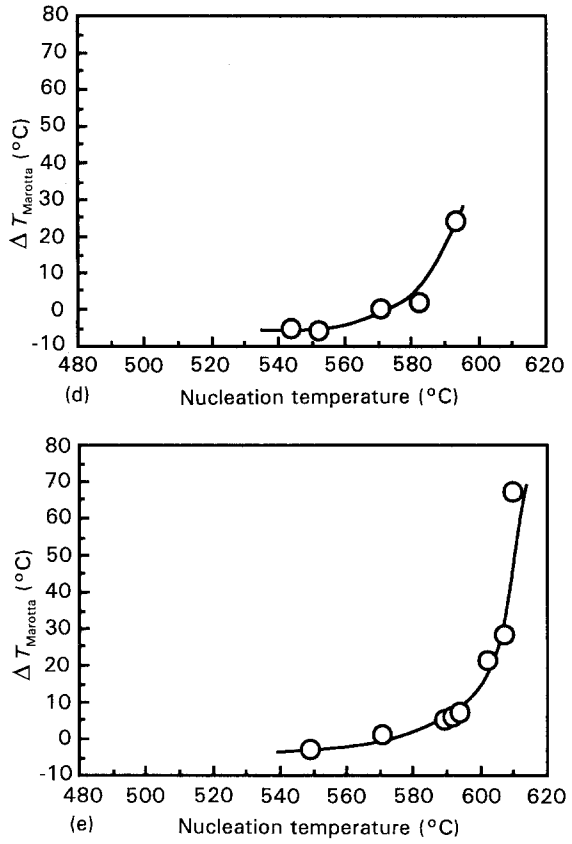

Figure 8 (continued).

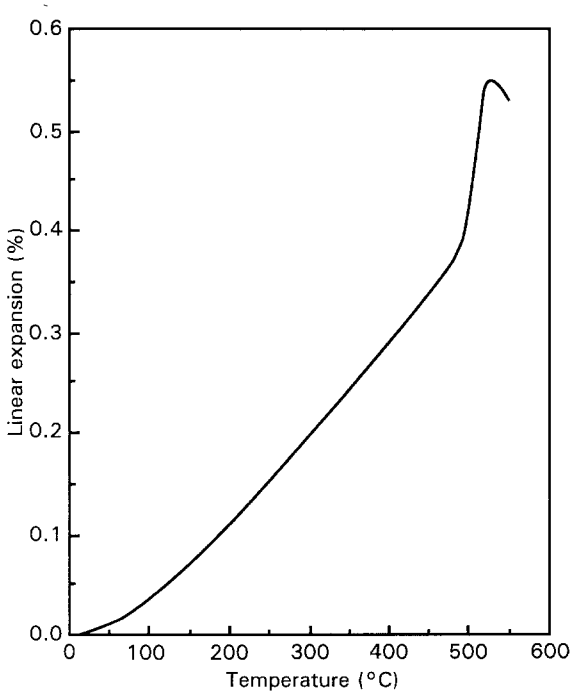

Figure 9 A representative dilatometer trace for a borate glass (Glass LB6).

ary. In the case of the Li_2O–B_2O_3 + 5 wt %SiO_2 ternary, this range is extended to beyond the $Li_2O \cdot 2B_2O_3$ boundary. Reference to Fig. 1 provides an approximate comparison [29] between the critical cooling rate for glass formation, R_c (which is a *quantitative* measurement of the GFA), and the reduced glass temperature, T_g/T_{liq}, for different values of the melt viscosity. The curve corresponding to a melt viscosity

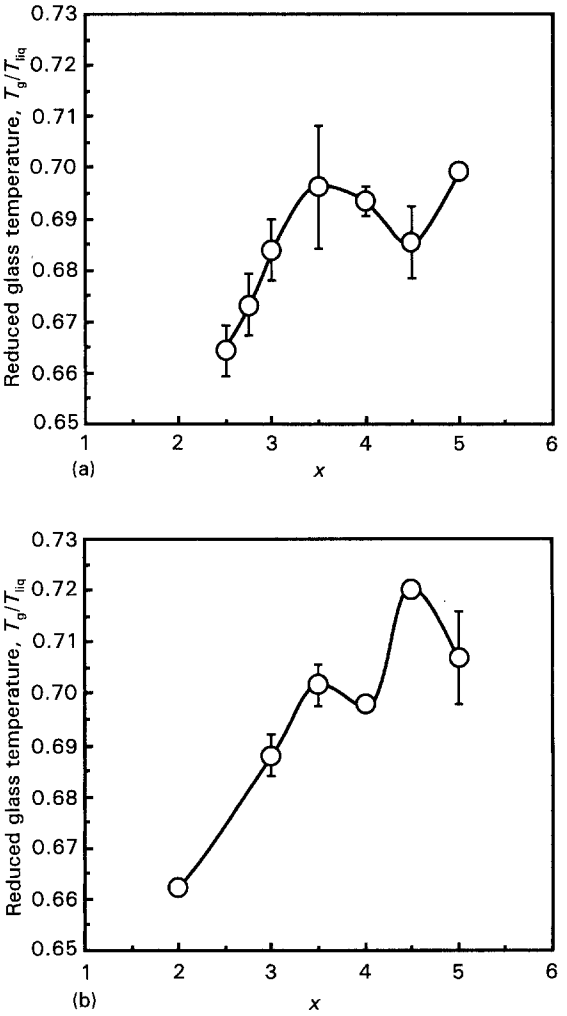

Figure 10 GFA plots (T_g/T_{liq}) as a function of the glass composition for: (a) $LiO \cdot xB_2O_3$, and (b) $Li_2O \cdot xB_2O_3$ + 5wt %SiO_2.

of $\sim 10^6$ Pa s relates to conventional silicate-based melts. The curve corresponding to ~ 10 Pa s relates more closely to less common glass-forming oxide melts, for example Bi_2O_3 based materials, whilst that for a melt viscosity of ~ 0.01 Pa s corresponds to many metallic melts. The other curve, corresponding to a melt viscosity of $\sim 10^4$ Pa s, approximates to borate melts. Using the data provided in Figs 1 and 10, it is possible to construct an R_c versus composition curve for the borate glasses, as shown in Fig. 21, which can be used as an approximate guide for estimating the critical cooling rate for glass formation for the borate glasses. The critical cooling rate for glass formation can be seen to vary over approximately one order of magnitude, between ~ 0.40 and 0.03 K s^{-1}, for these borate systems. The overall shape of the curve for the binary lithium borate glasses, with its minimum and maximum in R_c centred around $x \approx 3.5$ and 4.5, respectively, may reflect the variation in the viscosity with composition, as noted in the early work of Shartsis *et al.* [42]. The practical implication of the value of R_c is that, as a general rule, the smaller is the value of R_c, the thicker is the section of glass that can be produced in a single operation directly from the melt. For example, at one extreme, silica with $R_c \cong 10^{-4}$ K s^{-1} can be formed as a glass with a thickness approaching 1 m, whilst metallic Ni with

TABLE V Qualitative data for the glass-forming ability and for chemical-durability assessment

Glass code	Composition, x, for $Li_2O \cdot xB_2O_3$	Addition of SiO_2 (wt %)	Glass-forming ability[a]	Durability[b]
LB1	2	0	NGF	–
LB3	2.5	0	P/M	M
LB4	2.75	0	P/M	M
LB5	3	0	P/M	P
LB8	3.5	0	M/G	P
LB15	4	0	G	P
LB18	4.5	0	G	P
LB20	5	0	G	P
LB2	2	5	P/M	G
LB6	3	5	G	M/G
LB9	3.5	5	G	M
LB16	4	5	G	P
LB19	4.5	5	G	P
LB21	5	5	G	P

[a]NGF = not glass-forming; P = poor, $t < 5$ mm; M = moderate, $t < 5$–10 mm; G = good, $t > 10$ mm.
[b]P = poor, clouding of surface < 10 weeks; M = moderate, clouding < 25 weeks; G = good, no clouding < 52 weeks.

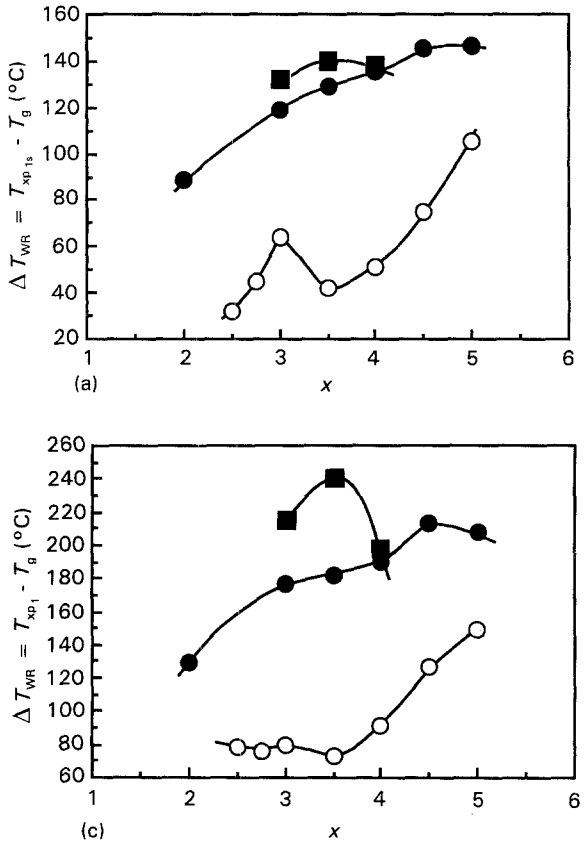

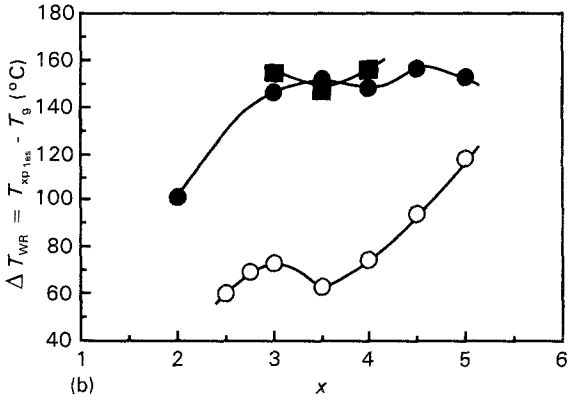

Figure 11 Thermal stability (working range, ΔT_{WR}) as a function of the glass composition for: (a) the peak start; (b) the extrapolated peak start, and (c) the peak crystallization temperatures; (For key, see Fig. 6.)

$R_c \approx 10^{10}$ K s^{-1} can only be formed in the amorphous state as very thin splatquenched foils ~ 0.1 μm thick. It has been shown in the present work for the LB6 lithium borate glass composition that a glass cylinder 38 mm in diameter and ~ 80 mm high can be cast crystal free. Using this information, and the derived R_c data it should be possible to predict the maximum thickness of glass that could be produced as a function of the glass composition; and this thickness could then be used to determine whether or not a given composition would be suitable for a specific application which requires a particular thickness of glass.

In practice, the thermal stability of a glass, and hence its working range, ΔT_{WR}, is also important in determining whether or not a given composition will

TABLE VI Quantitative chemical-durability data

Glass code	Environment	Temperature (°C)	Time (h)	Sample weight change (g)	Sample weight change (%)	Weight loss (10^{-3} mg mm^{-2} h^{-1})
LB6	Water	25	24	0.274	8.3	4.71
LB6	Water	25	48	0.483	14.8	4.19
LB6	Water	25	64	0.689	20.7	4.48

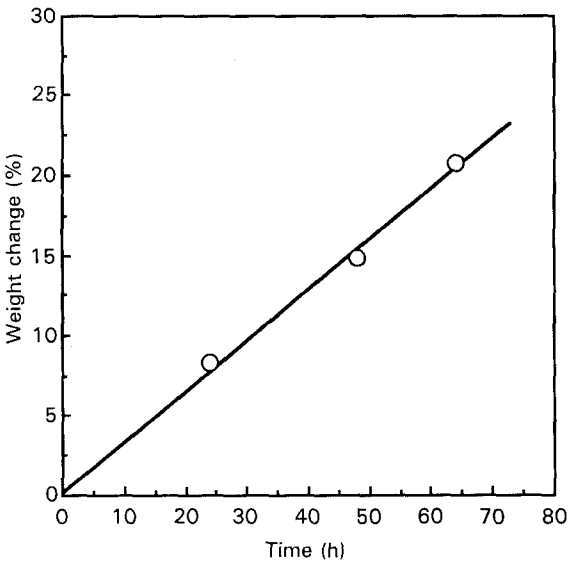

Figure 12 A chemical-durability plot for a borate glass (Glass LB6).

readily form a glass from the melt. The lithium borate glasses are thermally unstable, as illustrated by the DTA traces shown in Fig. 3, where the stability decreases as the B_2O_3 content decreases. The binary glasses are the least stable, exhibiting a single sharp crystallization peak. Addition of SiO_2 helps to stabilize the glasses, as can be seen from the broader crystallization peak obtained. Glass stability, as measured by the working range, increases in a complex non-linear manner with the B_2O_3 content, as depicted in Fig. 11. Hence, from the point of view of both the GFA *and* the glass stability, the higher-B_2O_3 content glasses are generally superior.

5.3. Chemical durability

Unfortunately, running counter to the trends in the GFA and in the thermal stability, the chemical durability of the lithium borate glasses decreases as the B_2O_3 content increases as is summarized in Tables V and VI. In the present work, as a compromise, glasses were chosen for further examination that exhibited a reasonable combination of both durability and GFA/stability, for example, $Li_2O \cdot 3B_2O_3$ + 5 %wt % SiO_2 and $Li_2O \cdot 3.5B_2O_3$ + 5%wt %SiO_2. The SiO_2 addition is extremely advantageous, in that it improves both the durability and the GFA simultaneously. Higher concentrations of SiO_2 would, of

TABLE VII Heat-treatment schedules and XRD results

Glass code	Heat-treatment schedule	Major crystal phases	Sample appearance
LB6	None	Amorphous	Transparent glass
LB6	1 h at 600 °C + 1 h at 700 °C	$LiB_3O_5 + Li_2B_4O_7$	White crystalline solid
LB6B	1 h at 600 °C + 1 h at 700 °C	$Li_2B_4O_7 + LiB_3O_5$	White crystalline solid

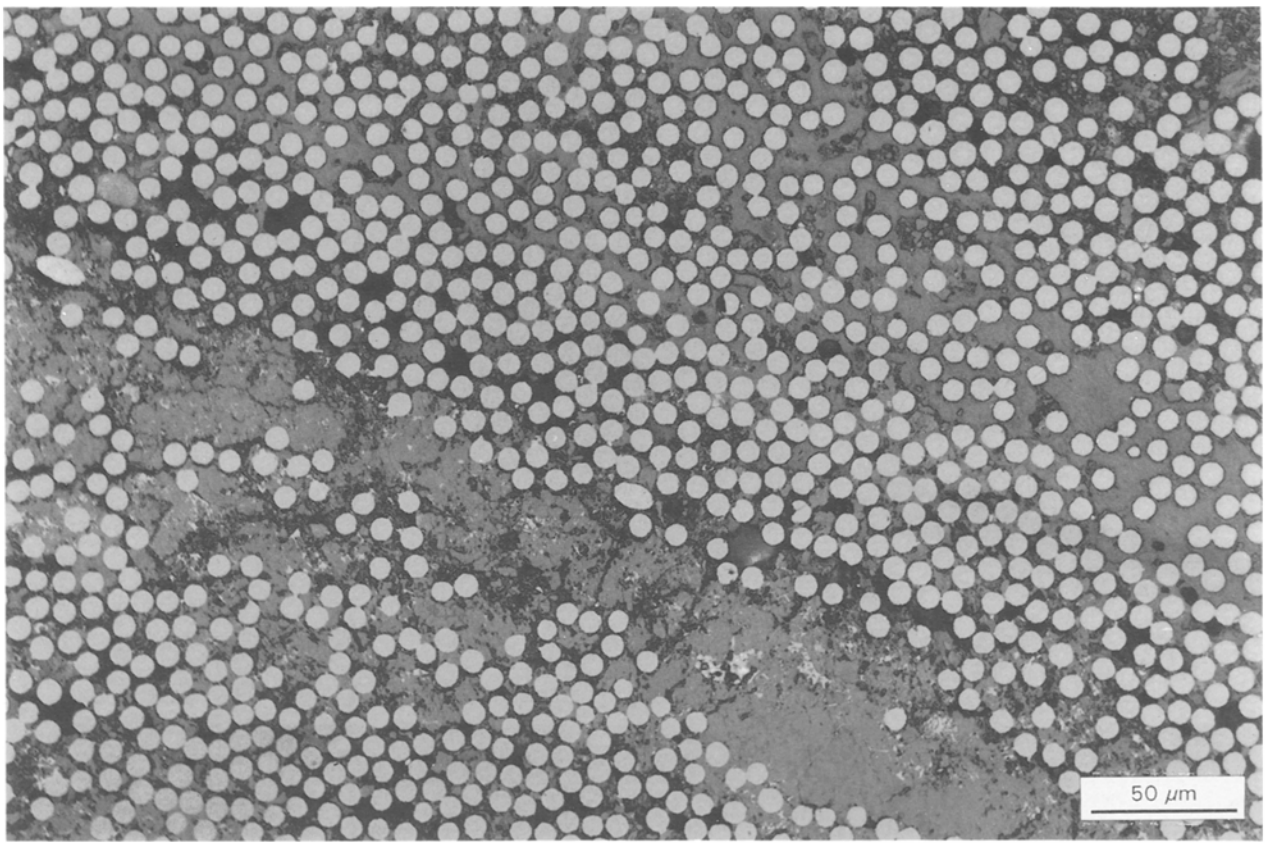

Figure 13 The microstructure of a carbon-fibre-reinforced lithium borate glass composite.

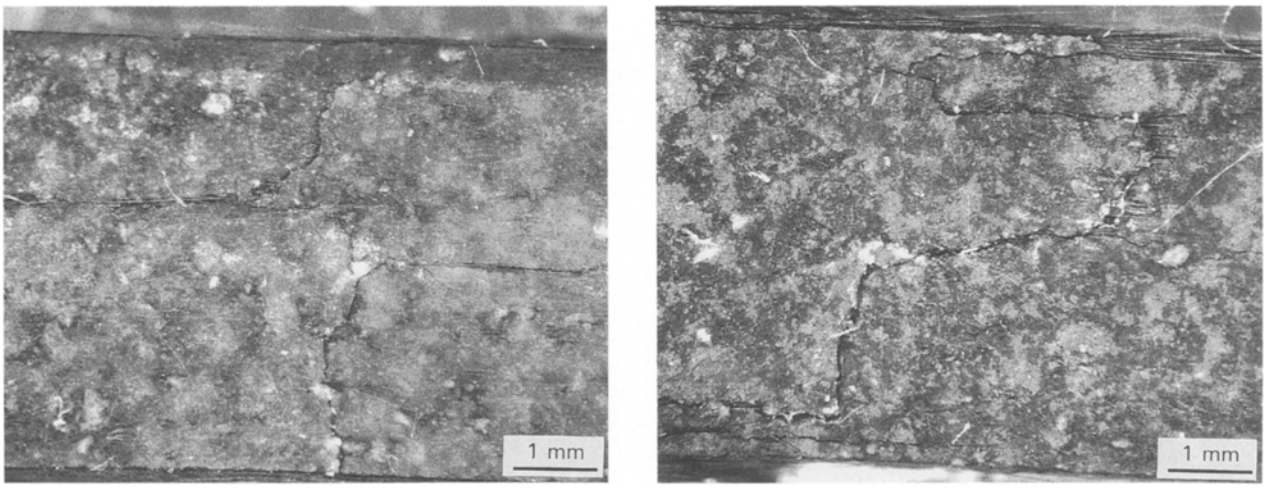

Figure 14 Fracture surfaces of carbon-fibre-reinforced lithium borate glass composites.

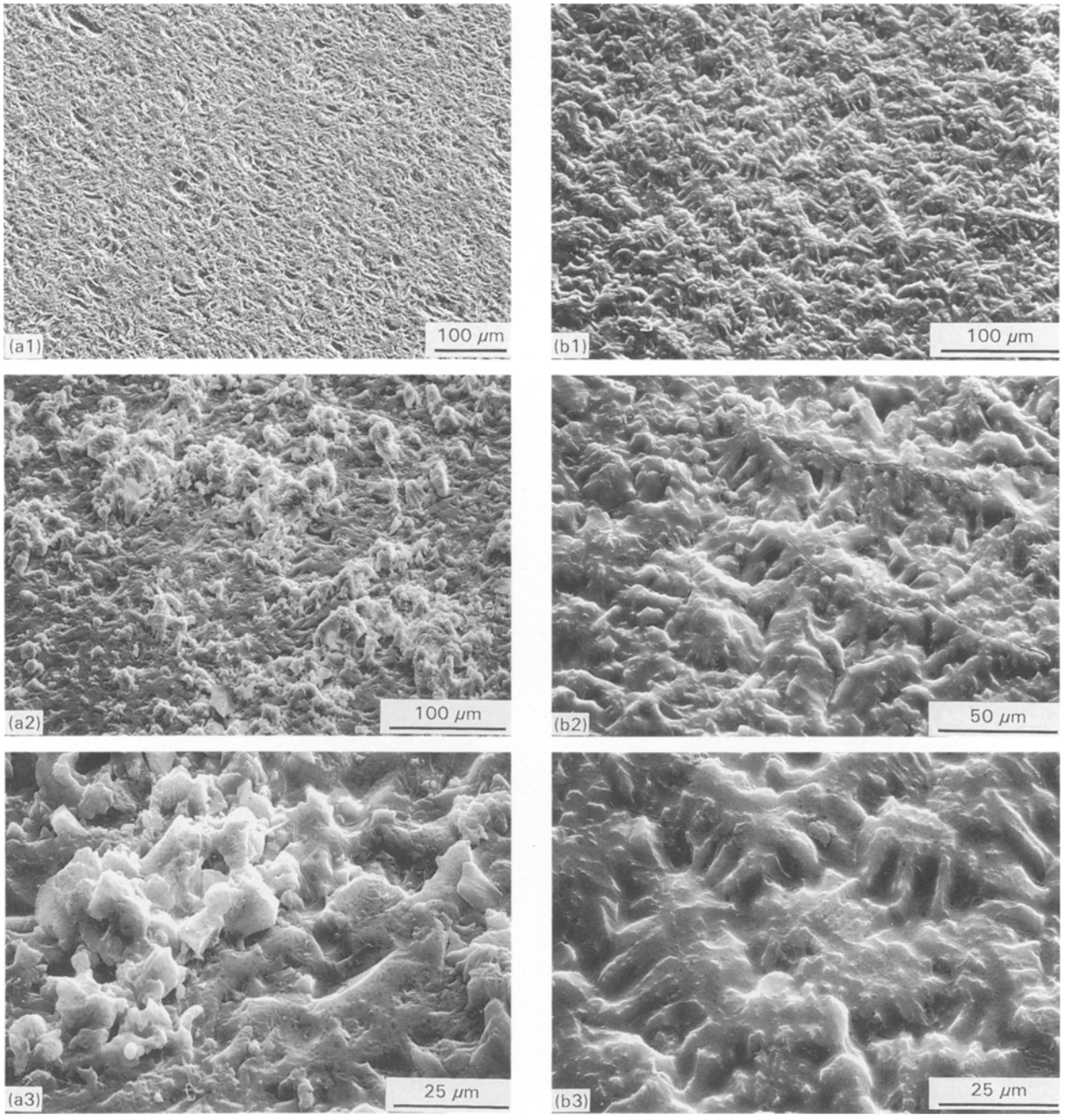

Figure 15 Micrographs of as-received and etched lithium borate glass surfaces:(a) as-machined, (b) etched in aqueous HF, (c) etched in water for 24 h and (d) etched in water for 64 h.

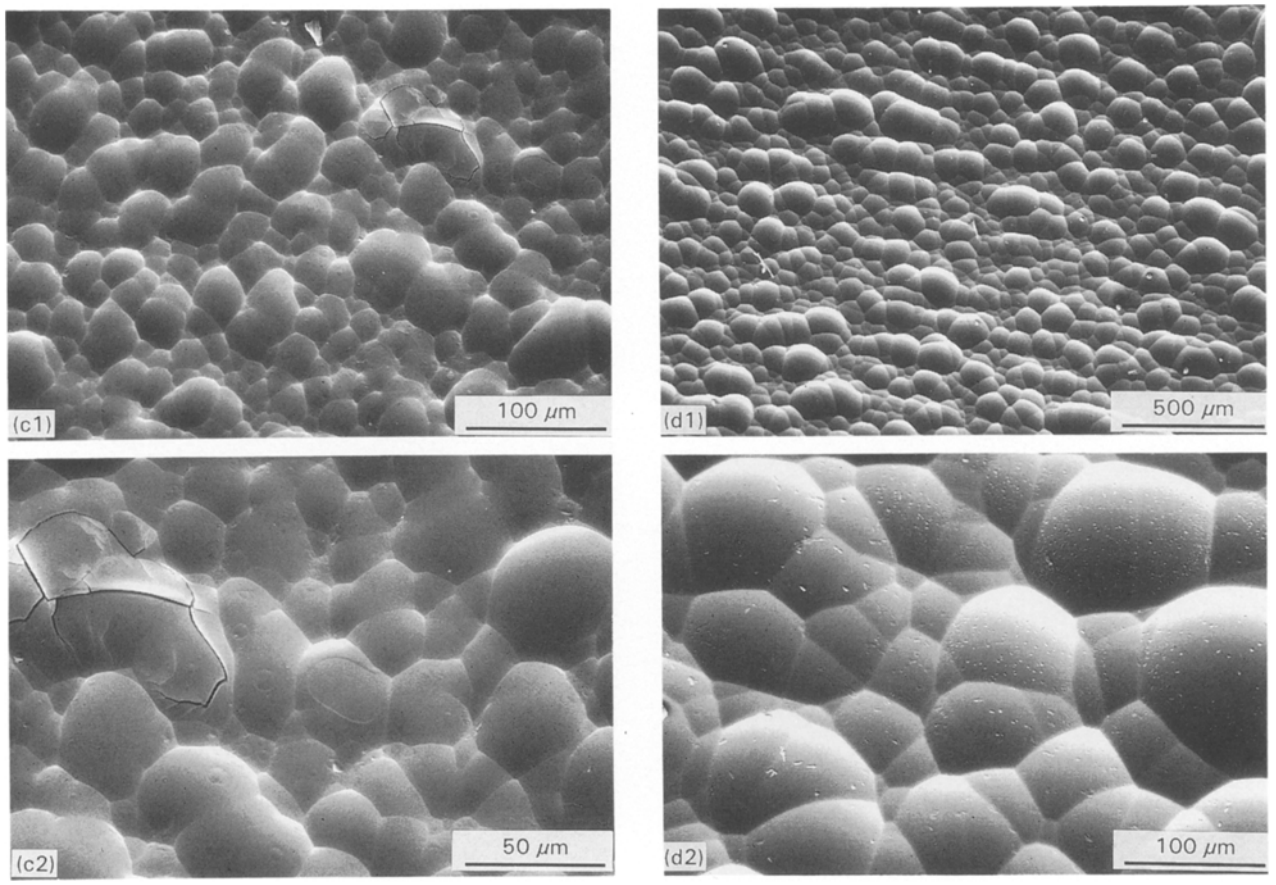

Figure 15 (continued).

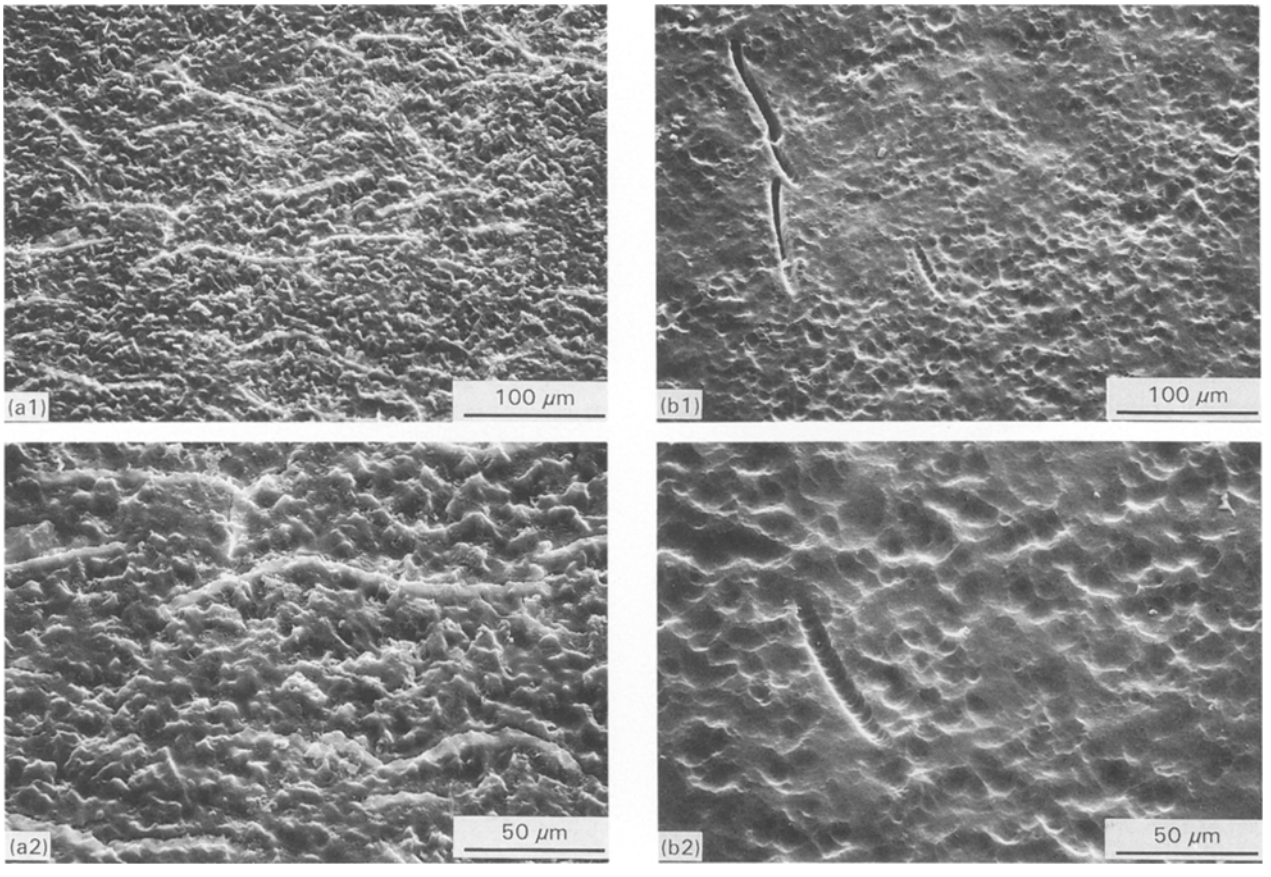

Figure 16 Micrographs of chemically ion-exchanged lithium borate glass surfaces: (a) ion-exchanged for $\frac{1}{2}$ h, (b) ion-exchanged for 4 h.

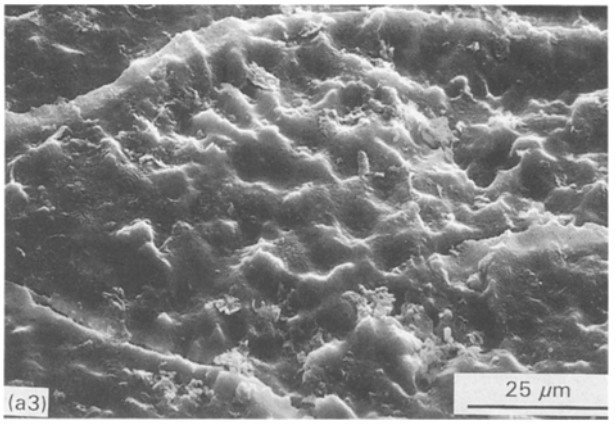

Figure 16 (continued).

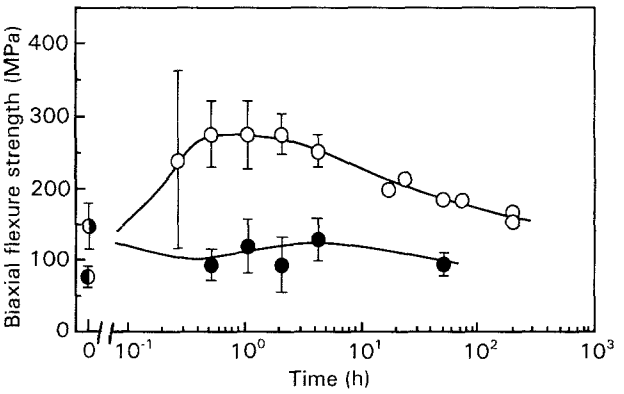

Figure 17 The biaxial flexure strength of lithium-borate glass as a function of the chemical-ion-exchange time (for glasses treated at 385 °C in: (o) $NaNO_3$, and (●) KNO_3, (◑) etched/untreated and (◐) as-machined/untreated.

TABLE VIII Biaxial flexure test results (Glass LB6)

Treatment conditions		Flexure strength (MPa)
Salt	Time at 385 °C	
$NaNO_3$	0.0	75 ± 13 (as-machined)
	0.0	155 ± 35 (etched)
	0.25	241 ± 110
	0.5	282 ± 32
	1.0	276 ± 45
	2.0	279 ± 25
	4.0	255 ± 10
	16.0	236
	23.0	253
	48.0	218
	72.0	218
	192.0	196
	193.0	183
KNO_3	0.5	94 ± 18
	1.0	120 ± 34
	2.0	94 ± 34
	4.0	130 ± 27
	49.0	94 ± 14

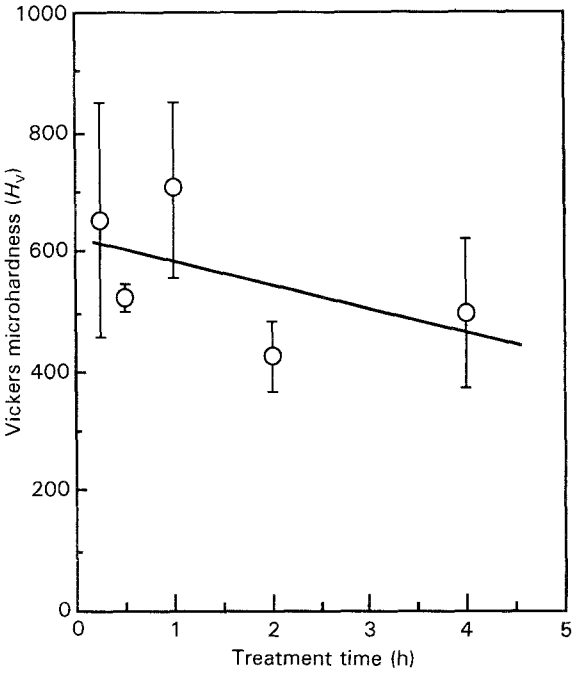

Figure 18 The microhardness of a lithium borate glass as a function of the chemical ion-exchange time (for glasses treated at 385 °C in $NaNO_3$).

course, be expected to improve these properties further.

5.4. Mechanical properties

The mean biaxial flexure strength of as-machined lithium borate glass discs is ~ 75 MPa, which is lower than that of typical silicate glasses (which have average values around 100 MPa). A number of potential strengthening methods were investigated in this work, with varying degrees of success, as outlined below.

Attempts at crystallizing the borate glasses in a controlled manner to produce fine-grained glass–ceramic materials with superior mechanical properties were not successful. As noted in Table IV, none of the additives summarized in Table I enhanced the nucleating efficiency, as measured by the difference in the crystallization temperature between the coarse and fine samples of glass. Similarly, the effect of isothermal heat-treatments on the crystallization behaviour of the glass indicates that heat treatment is not effective at promoting bulk crystallization, with the Marotta plots (Fig. 8) showing no evidence for enhanced nucleation. (The apparent increase in $\Delta T_{Marotta}$ at temperatures approaching T_x is due directly to partial surface crystallization of the samples during the heat treatment.). In addition, choice of a suitable heat treatment is rendered particularly difficult due to the low melting point lithium borate crystalline phases, as noted in the phase diagram (Fig. 20), with these low melting-point phases tending to exude from the bulk glass during heat treatment. In all cases, surface crystallization was predominant, and this gave rise to mechanically weak materials with coarse grain sizes and anisotropic properties.

Reinforcement of lithium borate glass with continuous unidirectionally aligned carbon fibres, on the other hand, was reasonably successful, since viable materials with useful properties were produced (for

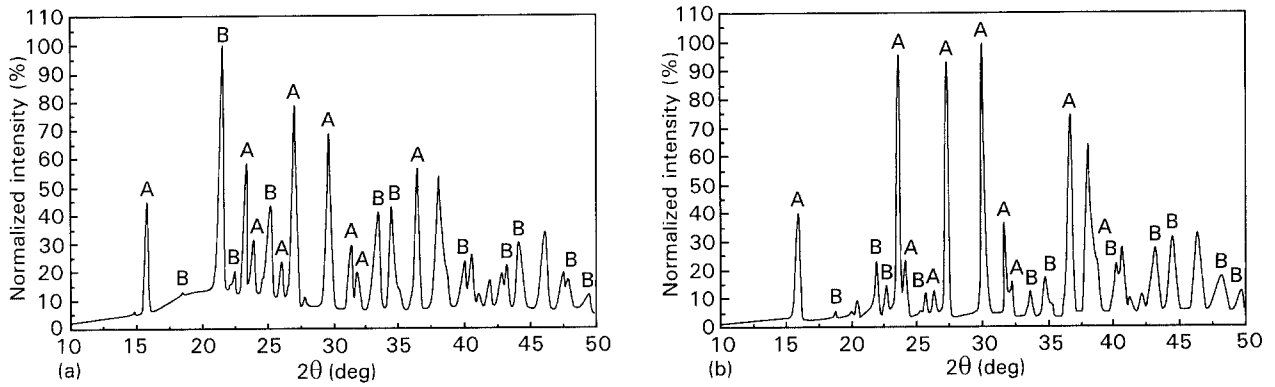

Figure 19 X-ray diffraction traces for crystallized glasses: (a) $Li_2O \cdot xB_2O_3$ + 5wt %SiO_2 + 1 mol % P_2O_5, (b)$Li_2O \cdot 3B_2O_3$ + 5wt %SiO_2. A = LiB_3O_5; B = $Li_2B_4O_7$.

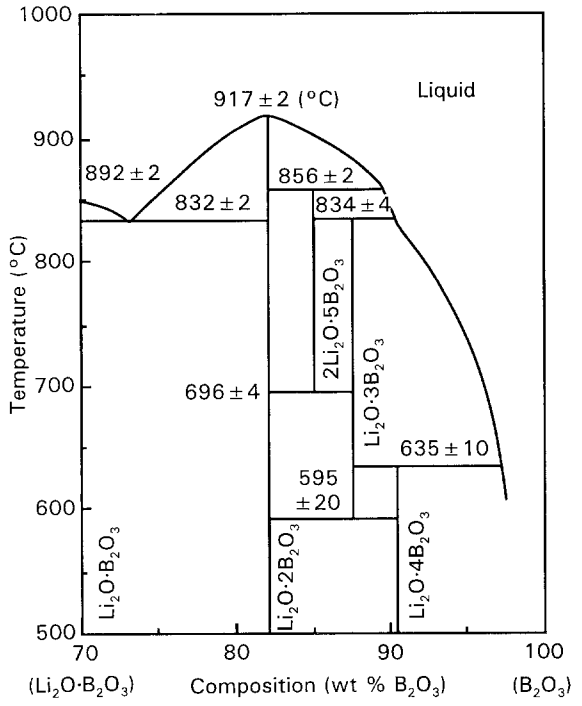

Figure 20 The binary Li_2O–B_2O_3 phase diagram (redrawn, with permission after [40]).

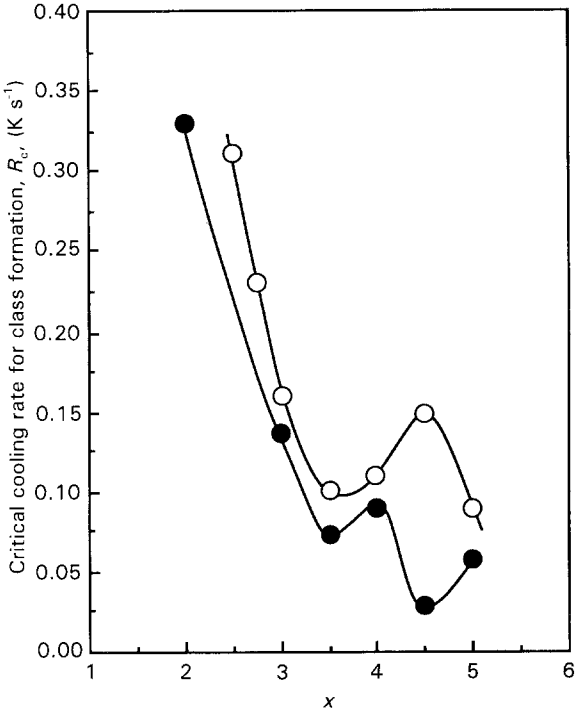

Figure 21 The estimated critical cooling rate for glass formation as a function of the borate-glass composition (○) $Li_2O \cdot xB_2O_3$, and (●) $Li_2O \cdot xB_2O_3$ + 5wt %SiO_2.

example, low density (1.75 g cm^{-3}), and moderate strength (144 MPa), together with an intermediate toughness (work of fracture = 4.2 kJ m^{-2}) coupled with a noncatastrophic failure mode). From a practical point of view, of course, composite materials are relatively expensive to produce.

The most successful method for increasing the strength of borate glass was undoubtedly chemical ion-exchange, as summarized in Table VIII and Fig. 17, with a maximum mean strength of ~ 280 MPa, a very high value for a borate system. As noted in Fig. 17, the overall behaviour of the chemically strengthened borate glass treated in sodium nitrate was superficially quite similar to the behaviour characteristic of silicate systems [41]; that is, there was a relatively large increase in the strength at short treatment times, followed by a gradual decrease from the maximum value at large times. (In the case of the borate glasses, the maximum strength was achieved at shorter treatment times than in the silicate glasses.) The fracture be-haviour of the treated borate glass was, however, very different, with samples breaking into a small number of large fragments, independently of the treatment time. (Silicate samples of similar thickness which were treated to yield similar strengths would be expected to fail in a frangible manner, and to produce a large number of small glass fragments.) Attempts at determining the stress profile for these materials were not successful, suggesting that the magnitude of the ion-exchange stresses is small. Additional information confirming that the depth of any compressive layer is likely to be small (that is, less than a few micrometres) was provided by light abrasion of a treated borate glass surface which reduced the strength to the value noted for the untreated materials. In addition, in contrast to the samples treated in the sodium salt, no improvement in the strength was observed when the samples were treated with potassium

nitrate. If the strengthening mechanism was a simple exchange of larger ions for smaller ions, a further improvement in strength would have been expected over that obtained for the exchange of Na^+ ions for Li^+ ions. As noted in Fig. 17, this is clearly not the case. The strengthening mechanism for the borate glass is therefore less clear, and it may be due to a combination of factors, including the more effective removal of surface flaws by the action of the molten salt.

Although the strength of the borate glass can also be improved significantly simply by etching in aqueous HF, or even in pure water, the improvement in strength is only transitory, since light abrasion quickly reduces the strength to that of the untreated values. To retain the high strength values that can be achieved by surface treatment of the borate glass, it would be necessary to coat the glass with a compatible abrasion-resistant coating. Coating methods were not examined in this work.

6. Conclusions

1. Binary lithium borate glasses were successfully prepared as bulk samples several millimetres thick containing up to ~ 29 mol% Li_2O. The Li_2O content can be increased to ~ 33 mol % by incorporation of 5 wt % SiO_2.

2. The glass-forming ability (GFA) and the glass thermal stability increased as the B_2O_3 content increased. The critical cooling rate for glass formation has been estimated to vary between ~ 0.03–$0.40\ K\ s^{-1}$ for the binary lithium borate materials for Li_2O contents between 17 and 33 mol %.

3. Counter to the behaviour of the GFA and the thermal stability, the chemical durability decreased as the B_2O_3 content increased.

4. Small additions of SiO_2 (for example, 5 wt %) substantially improved the GFA, the thermal stability and the chemical durability of the lithium borate glasses.

5. A useful compromise composition combining a reasonable GFA, thermal stability and chemical durability is given by $Li_2O \cdot (3 \text{ or } 3.5)B_2O_3 +$ 5 wt %SiO_2.

6. Attempts at crystallizing lithium borate glass in a controlled manner to produce high-strength borate glass–ceramics analogous to conventional silicate glass–ceramic materials were not successful.

7. Reinforcement of lithium borate glass with carbon fibres was successful in producing moderately high-strength materials with useful fracture toughnesses coupled with a non-catastrophic failure mode (flexural strength = 144 MPa; work of fracture = $4.2\ kJ\ m^{-2}$).

8. Etching in aqueous HF or pure water produced a moderate strengthening effect (up to 155 MPa), but this improvement in strength was easily lost through light abrasion.

9. Treatment in molten sodium nitrate (but not potassium nitrate) improved the mechanical strength of lithium borate glass very substantially (up to a maximum mean strength of ~ 280 MPa). This improvement in strength was, however, lost by light abrasion. This strongly suggests that the mechanism of strengthening for these glasses is not by simple ion-exchange (and it is therefore not analogous to the mechanism in silicate glasses): it is more probably due to a more effective removal of surface flaws than can be achieved by etching alone.

Acknowledgements

The authors are grateful to Mr J. C. Ruckman at AWE, for providing SEM photographs of the samples and to Mrs. E. A. Prior at AWE for providing the optical micrographs. We also wish to thank Mr. M. R. Clay, at AWE for carrying out the X-ray diffraction (XRD) work and for the interpretation of the XRD data. This work was supported by the Procurement Executive to the Ministry of Defence. This paper is published with the permission of the controller of Her Britannic Majesty's Stationery Office under British Crown Copyright 1994/MOD.

References

1. D. L. GRISCOM, in "Borate glasses: structure, properties and applications", edited by L. D. Pye, V. D. Rréchette and N. J. Kreidl (Plenum Press, New York, 1978) pp. 11–138.
2. S. A. FELLER, W. J. DELL and P. J. BRAY, *J. Non-Cryst. Solids* **51** (1982) 21.
3. N. J. KREIDL in "Glass science and technology", Vol. 1, edited by D. R. Uhlmann and N. J. Kreidl, (Academic Press, New York, 1983) pp. 105–299.
4. M. SHIBATA, C. SANCHEZ, H. PATEL, S. FELLER, J. STARK, G. SUMCAD and J. KASPER, *J. Non-Cryst. Solids* **85** (1986)29.
5. P. J. BRAY, in "Defects in glasses", edited by F. L. Galeener, Materials Research Society Symposium Proceedings Vol. 61 (Materials Research Society, 1986) pp. 121–133.
6. N. J. KREIDL, *Glastech. Ber.* **60** (1987) 249.
7. G. D. CHRYSSIKOS, E. I. KAMITSOS and M. A. KARAKASSIUDES, *Phys. Chem. Glasses* **31** (1990) 109.
8. T. TAKAMORI, in "Treatise on materials science and technology" Vol. 17, edited by M. Tomozawa and R. H. Doremus, (Academic Press, New York, 1979) pp. 173–255.
9. I. W. DONALD, *J. Mater. Sci.* **28** (1993) 2841.
10. H. L. TULLER, D. P. BUTTON and D. R. UHLMANN, *J. Non-Cryst. Solids* **40** (1980) 93.
11. M. DEVAUD, J-Y. PRIEUR and W. D. WALLACE, *Solid State Ionics* **9 & 10** (1983) 593.
12. N. J. KREIDL, *Bull. Amer. Ceram. Soc.* **63** (1984) 1394.
13. M. D. INGRAM, *Phys. Chem. Glasses* **28** (1987) 215.
14. Y. KUTOMI, A. TOMITA and N. TAKEUCHI, *J. Mater. Sci. Lett.* **6** (1987) 301.
15. I. W. DONALD, *J. Mater. Sci.* **24** (1989) 4177.
16. P. W. MCMILLAN, "Glass ceramics" (Academic Press, London, 1979).
17. I. W. DONALD, "Glass ceramics – an update", Encyclopedia of Materials Science and Engineering: Supplementary Vol. 3 (Pergamon Press, Oxford, 1993), pp. 1689–1695.
18. S. SIMON and A. L. NICULA, *Phys. Status Solidi.* **81** (1984) K1–K5.
19. M. F. FAHMY and K. N. SUBRAMANIAN, *Phys. Chem. Glasses* **28** (1987) 1.
20. *Idem. ibid.* **28** (1987) 49.
21. G. L. SMITH, G. F. NEILSON and M. C. WEINBERG, *ibid.* **28** (1987) 257.
22. M. MAEDA and T. IKEDA, *J. Phys. Chem. Solids* **49** (1988) 35–39.
23. A. A. GOKTAS, G. F. NIELSON and M. C. WEINBERG, *J. Mater. Sci.* **27** (1992) 24–28.

24. R. L. THAKUR and S. THIAGARAJAN, *Glass Ceram. Bull.* **13** (1966) 33.
25. A. MAROTTA, A. BURI and F. BRANDA, *J. Mater. Sci.* **16** (1981) 341–344.
26. A. MAROTTA, S. SAIELLO, F. BRANDA and A. BURI, *Verres Réfract.* **35** (1981) 477–480.
27. S. SAIELLO, F. BRANDA, A. BURI and A. MAROTTA, *ibid.* **36** (1982) 859–861.
28. A. MAROTTA, A. BURI, F. BRANDA and S. SAIELLO, in "Advances in ceramics", Vol. 4, edited by J. H. Simmons, D. R. Uhlmann and G. H. Beall (American Ceramic Society, Columbus, 1982) pp. 146–152.
29. H. A. DAVIES, *Phys. Chem. Glasses* **17** (1976) 159–173.
30. M. J. C. HILL, Atomics Weapons Establishment, unpublished work (1989).
31. W. BRADSHAW, *J. Mater. Sci.* **14** (1979) 2981–2988.
32. I. W. DONALD and M. J. C. HILL, *ibid.* **23** (1988) 2797–2809.
33. M. J. C. HILL and I. W. DONALD, *Glass Technol.* **30** (1989) 123–127.
34. F. F. VITMAN and V. P. PUKH, *Indust. Lab.* **29** (1963) 925–930.
35. J. B. WACHTMAN, W. CAPPS and J. MANDEL, *J. Mater.* **7** (1972) 188–194.
36. ASTM F 394–78 (1978)802–808.
37. J. E. RITTER, K. JAKUS, A. BATAKIS and N. BANDYOPADHAY, *J. Non-Cryst. Solids* **38 & 39** (1980) 419–424.
38. J. E. SHELBY, *J. Amer. Ceram. Soc.* **66** (1983) 225.
39. M. AFFATIGATO, S. FELLER, E. J. KHAW, D. FEIL, B. TEOH and O. MATHEWS, *Phys. Chem. Glasses* **31** (1990) 19.
40. B. S. R. SASTRY and F. A. HUMMEL, *J. Amer. Ceram. Soc.* **42** (1959) 218.
41. I. W. DONALD, M. J. C. HILL, B. L. METCALFE, D. J. BRADLEY and A. D. BYE, *Glass Technol.* **34** (1993) 114.
42. L. SHARTSIS, W. CAPPS and S. SPINNER, *J. Amer. Ceram. Soc.* **36** (1953) 319.

Received 25 April
and accepted 7 June 1994